



Visualization and characterization of *Enterococcus faecalis* biofilm structure in bovine dentin using 2D and 3D microscopic techniques

Ali Keleş¹ · Cangül Keskin¹ · Melis Kalkan² · Yusuf Yakupoğulları³ · Mehmet Gül⁴ · Hikmet Aydemir¹ · Fikretin Şahin²

Received: 24 April 2020 / Revised: 11 August 2020 / Accepted: 2 September 2020 / Published online: 11 September 2020
© Springer-Verlag GmbH Germany, part of Springer Nature 2020

Abstract

Bacterial biofilms are related to various dental and periodontal infectious diseases, and the characterization of this biological structure with micro-computed tomography (micro-CT) may offer valuable information for clinical and research applications. In this study, we aimed to develop a model to visualize three-dimensionally the biofilm structure on dentin using micro-CT. Dentin blocks were prepared and incubated in tryptic soy broth with *Enterococcus faecalis* (ATCC 29212). The control group did not receive any staining procedure, while groups 1 and 2 were stained with 100% and 50% barium sulfate, respectively. Transmission electron microscopy (TEM) and confocal laser scanning microscopy (CLSM) were used to detect biofilm formation, barium sulfate penetration, and microbial cell density in the biofilm. Micro-computed tomography (micro-CT) (SkyScan 1172, Bruker Co., Belgium) was used to visualize biofilm formation on the dentin blocks. Biofilm thicknesses were measured from 10 different locations on the specimen surfaces, using CTAn v.1.14.4 software. Obtained data were statistically analyzed using Kruskal–Wallis and Dunn’s tests. TEM photomicrographs showed that barium sulfate could penetrate the biofilm structure. CLSM analysis showed that viable and total cell densities were similar between the control and barium sulfate-treated groups ($P > 0.05$), indicating barium sulfate had no significant influence on cell density. In barium sulfate-treated blocks, biofilm could be discriminated from the dentin, and its thickness could be measured with micro-CT. This study showed that bacterial biofilm on dentin could be characterized by micro-CT after barium sulfate staining without causing any significant side effect on viable and total cell densities.

Keywords Biofilm · Dentin · Micro-computed tomography · Transmission electron microscopy

Introduction

Biofilms are complex polymicrobial structures, which are composed of microbial cells enclosed in a self-produced extracellular polymeric matrix adherent to a surface

Communicated by Erko stackebrandt.

✉ Cangül Keskin
cangul.keskin@gmail.com; cangul.keskin@omu.edu.tr

Ali Keleş
alikeles29@yahoo.com

Melis Kalkan
meliskalkann@gmail.com

Yusuf Yakupoğulları
yusuf.yakupogullari@inonu.edu.tr

Mehmet Gül
mehmet.gul@inonu.edu.tr

Hikmet Aydemir
hikmetaydemir@omu.edu.tr

Fikretin Şahin
fsahin@yeditepe.edu.tr

¹ Department of Endodontics, Faculty of Dentistry, Ondokuz Mayıs University Samsun, Samsun, Turkey

² Department of Genetic and Bioengineering, Faculty of Engineering and Architecture, Yeditepe University, Istanbul, Turkey

³ Department of Medical Microbiology, Faculty of Medicine, İnönü University, Malatya, Turkey

⁴ Department of Histology and Embryology, Faculty of Medicine, İnönü University, Malatya, Turkey

(Felmming and Wingender 2010). Oral cavity accommodates an environment for microorganisms to colonize, proliferate, and to form biofilms. Microorganisms are implicated in the pathogenesis of a wide range of oral diseases, including caries, periodontal infections, and apical periodontitis (Kreth and Herzberg 2015). Biofilms were shown to be responsible for 80% of such infections since the bacterial biofilms are 1,000 times more resistant to antimicrobials than planktonic cells (Costerton et al. 1999; Stewart and Costerton 2001). Therefore, a thorough understanding of oral infectious diseases must include comprehensive biofilm studies. Proper characterization of the bacterial biofilms on dentin requires cost- and labor-intensive techniques, such as scanning electron microscopy (SEM), transmission electron microscopy (TEM), environmental scanning electron microscopy, atomic force microscopy and fluorescence in situ hybridization (Hannig et al. 2010). Electron microscopic methods provide detailed visualization of biofilm; however, quantification is difficult, and specimens are subjected to irreversible processes including fixation, dehydration, and coating. Environmental scanning electron microscopy was utilized to overcome the limitations of the preparation process but provided limited three-dimensional visualization (Bergmans et al. 2005; Hannig et al. 2010). Though TEM has been regarded as the gold standard in electron microscopy due to its high-resolution rate down to 0.1 nm, TEM also requires an extensive preparation process, which renders the specimen useless for further evaluation (Bergmans et al. 2005; Hannig et al. 2010). All these techniques described above could detect biofilm presence, but they fail to use the same specimen in the following procedures to determine the effect of elimination protocols on biofilm structures.

Micro-computed tomography is a rapidly developing technology that utilizes X-rays and produces 3D images of particles at the micrometer scale with their inner structure. Micro-CT characterizes the structures depending on differences of the X-ray absorption values of the components, which are related to atomic number and density values (Rolland du Roscoat et al. 2014). Unlike the techniques mentioned previously, micro-CT is a non-destructive technique that enables specimens to be used after scanning for further experimental processes (Ordinola-Zapata et al. 2017). Additionally, since destructive sample preparation steps that can influence the microstructure are not required, the micro-CT is capable of showing structures accurately as closest to their natural state. The ability of micro-CT to visualize microbial biofilm has gained popularity recently. Different media to grow biofilm on and contrasting agents were investigated in previous studies, which suggested that micro-CT is promising for quantitative evaluation of biofilm structure (Carrel et al. 2018; Davit et al. 2011; Ivankovic et al. 2016; Pires et al. 2018; Rolland du Roscoat et al. 2014). Four of those

studies advocated the use of different contrasting agents to differentiate biofilm structure from surrounding structures with similar X-ray absorption properties (Carrel et al. 2018; Davit et al. 2011; Ivankovic et al. 2016; Rolland du Roscoat et al. 2014). Barium sulfate is one of the most commonly used contrasting agents during CT examinations due to its radiopaque nature. The suspension is also non-toxic because of its insolubility in water, is low-cost, does not diffuse within the tissues and provides high density radiographs (Davit et al. 2011; Plouraboue et al. 2004). Micro-CT visualization of biofilm formation on dentin structure using barium sulfate as a contrasting agent might aid in the quantitative evaluation of certain disinfecting procedures on biofilm without harming the specimens. Therefore, the present study aimed to assess the efficacy of micro-CT to visualize *Enterococcus faecalis* biofilm on dentin three-dimensionally in comparison with TEM and confocal laser scanning microscopy (CLSM) and to provide a quantitative method to analyze biofilm structure attached to dentin. The null hypothesis would be that micro-CT could visualize *Enterococcus faecalis* biofilm structured on dentin blocks.

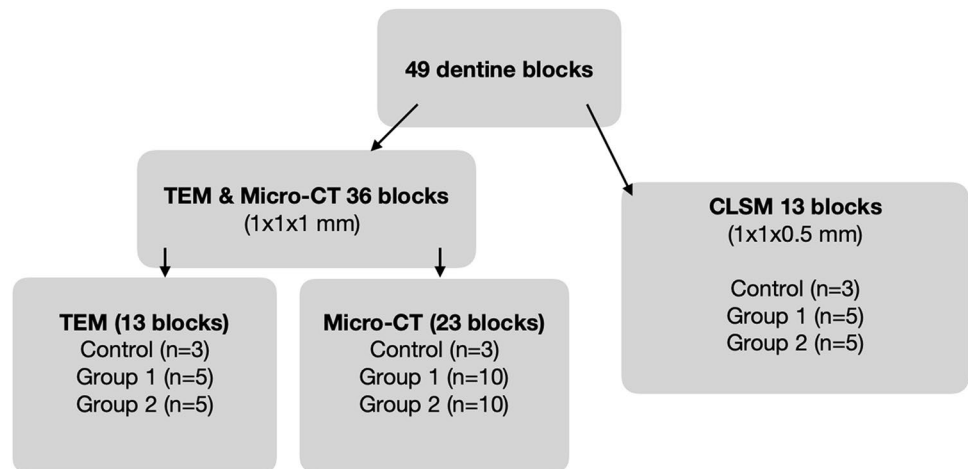
Materials and methods

Preparation of dentin blocks and biofilm formation

A total of 36 dentin blocks from bovine teeth with $1 \times 4 \times 1$ mm dimensions were prepared for TEM and micro-CT analyses, and 13 dentin blocks with $1 \times 4 \times 0.5$ mm dimensions were prepared for CLSM analysis using high-speed saw underwater cooling (Isomet 5000, Buehler, Lake Bluff, IL, USA) (Fig. 1). Thirteen dentin blocks with $1 \times 4 \times 1$ mm dimensions were selected for TEM analysis, whereas the remaining 23 blocks were used for micro-CT imaging. Dentin blocks were immersed in 2 mL of 5.25% sodium hypochlorite for 5 min and subsequently into 2 mL of 17% EDTA for 1 min to remove smear layer on them and then they were immersed in 5% sodium thiosulfate for 5 min to neutralize the effect of sodium hypochlorite. Dentin blocks were then dried and irradiated with UV light for 20 min.

E. faecalis strains (ATCC 29212) were incubated at 37 °C in 15 mL tryptic soy broth (TSB-T8907 Sigma-Aldrich) for 24 h as described in previous studies (Du et al. 2014; Rosen et al. 2016). Optical density was determined as 0.5 by 1:14 dilution with TSB measured at 600 nm using a spectrophotometer (UV Spec 1800 Shimadzu, Japan) resulting a 10^5 cfu/mL bacterial concentration. Each block was transferred into sterile 24-well plates within a biological safety cabinet. Each well was filled with 1800 μ L TSB and 200 μ L bacterial suspension and incubated at 37 °C for 48 h.

Fig. 1 Schematic representation of the distribution of specimens according to the visualization techniques. Specimens that were not stained with barium sulfate were categorized as the control group. Groups 1 and 2 were stained with 100% and 50% barium sulfate, respectively



Barium sulfate staining

Inoculant was collected completely and flushed with sterile phosphate-buffered salt (PBS) solution three times to remove the medium. Nine dentin blocks (6 of them with $1 \times 4 \times 1$ mm, and 3 of them with $1 \times 4 \times 0.5$ mm dimensions), which were not treated with barium sulfate, were used as control groups for each visualization technique ($n=3$). Wells containing these blocks were only filled with sterile PBS and not stained. The wells of 20 blocks (15 of them with $1 \times 4 \times 1$ mm, and 5 of them with $1 \times 4 \times 0.5$ mm dimensions) were filled with 2 mL 100% barium sulfate solutions (R-X suspension 100%, Ankara, Turkey) (1 g/mL concentration) constituting Group 1. In Group 2, the wells of the remaining 20 blocks (15 of them with $1 \times 4 \times 1$ mm, and 5 of them with $1 \times 4 \times 0.5$ mm dimensions) were filled with 2 mL 50% (0.5 g/mL) barium sulfate solution. All dentin blocks within wells were incubated at 37 °C 24 h.

Transmission electron microscope evaluation

Three dentin blocks, which were not stained with barium sulfate, were utilized as a control group. In groups 1 and 2 ($n=5$), the excess barium sulfate was removed from the surface of dentin blocks. The dentin blocks were fixed with 2.5% glutaraldehyde and decalcified using RDO-Gold Decalcifier (Electron Microscopy Sciences, Hatfield, PA). Following the decalcification, the dentin blocks were fixed with 1% osmium tetroxide and dehydrated using acetone and embedded in resin blocks (Araldite 502). 80 nm sections were prepared from Araldite blocks using ultramicrotome on copper grids. Sections on copper grids were treated with uranyl acetate for contrasting, and photomicrographs were taken using Zeiss Libra 120 TEM (Carl Zeiss, Oberkochen, Germany).

Confocal laser scanning microscopy evaluation

Five specimens were prepared for each group 1 and 2. Blocks that were not incubated with barium sulfate solution were used as the control group ($n=3$). The excess barium sulfate on the dentin blocks was removed by washing three times with 1X sterile PBS. SYTO 9 Green Fluorescent Nucleic Acid Stain (ThermoFisher Scientific S34854) and Propidium Iodide (ThermoFisher Scientific P3566) dyes were formed by mixing 1 μ L of each with 1 mL of distilled water. 200 μ L of both dyes at 1:1000 concentrations was added onto the dentin blocks and allowed to incubate for 20 min at room temperature in a dark environment.

Images obtained by CLSM (Carl Zeiss Microscopy System LSM700, Germany) were analyzed using the ZEN 2.3 (Carl Zeiss Microscopy GmbH, Germany) program. To establish standardization on the evaluated area, a square-shaped area with 100- μ m square in the middle of the CLSM images was selected (Fig. 2). Viable cell density and total cell density in this 100- μ m square area were calculated via Zeiss ZEN 2.3 software (Carl Zeiss, Oberkochen, Germany) by calculating irradiated green and red areas and their densities were recorded in airy unit (AU).

Micro-computed tomography scanning and analysis

For micro-CT imaging, three specimens, which were not stained with barium sulfate were used in the control group ($n=3$), whereas 20 stained specimens were selected for groups 1 and 2 ($n=10$). The excess barium sulfate on the dentin blocks was removed by washing three times with 1X sterile PBS. Each dentin block was fixed using sticky wax and scanned using the micro-CT system (SkyScan 1172; Bruker-microCT, Kontich, Belgium), which was operated at 80 kV and 124 μ A. Scanning was performed with 2.46 μ m isotropic resolution at 180° rotations around

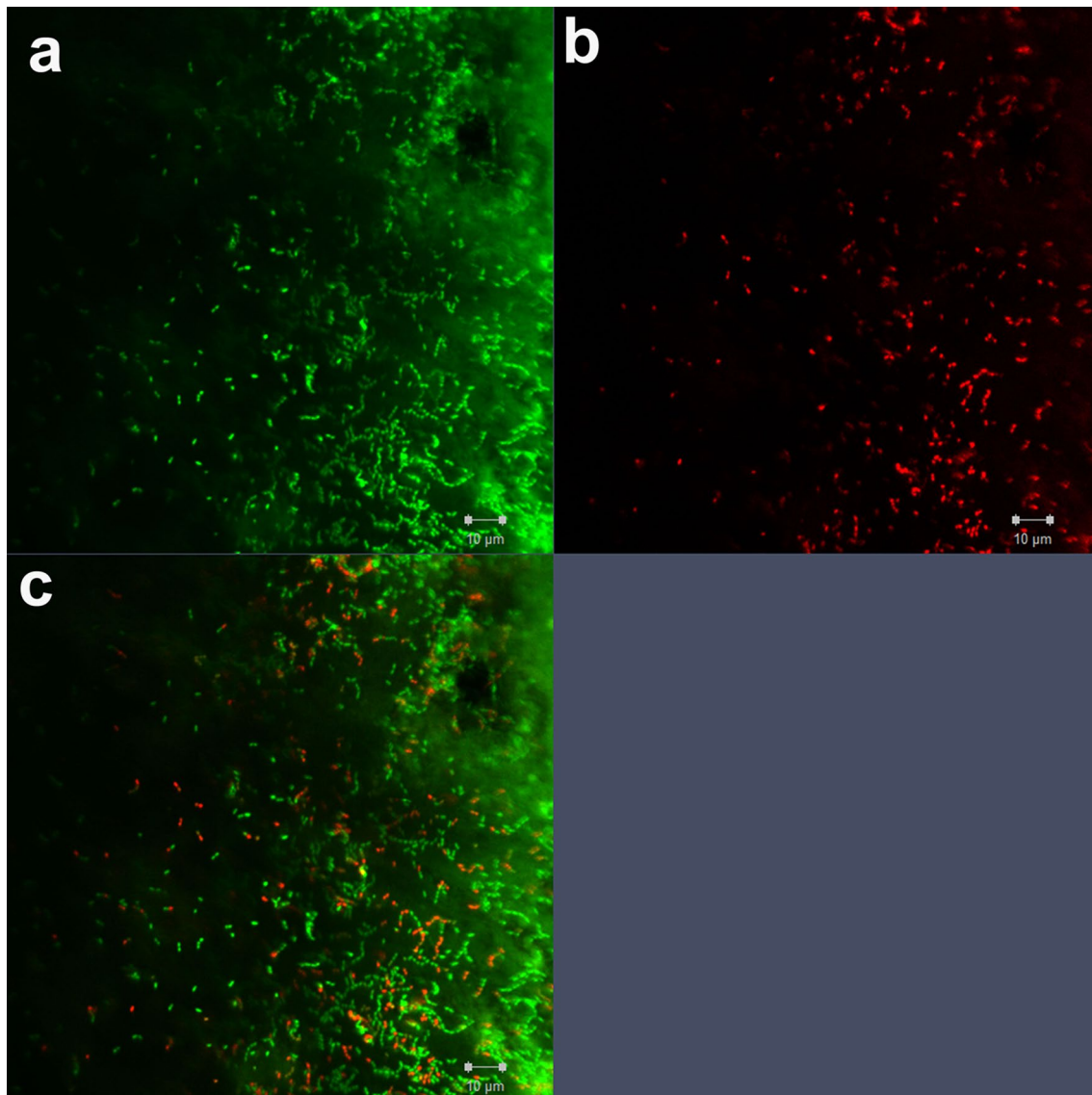


Fig. 2 A standardized area with 100- μ m square dimensions was selected in the center of the CLSM images, and cell densities were calculated within this area (a–c). Bacteria were stained with green

fluorescent SYTO 9 (a) and red fluorescent Propidium iodide (b). The staining caused viable cells to appear green and dead cells appearing red under CLSM (c)

the vertical axis with a camera exposure time of 1600 ms and a rotation step of 0.4° for 1 h. X-rays were filtered with 500 μ m aluminum filters. Data were reconstructed using NRecon software (v. 1.6.9, Bruker-microCT) with beam-hardening correction of 45%, smoothing of 2, and an attenuation coefficient range of 0–0.06. Biofilm thickness was measured using CTAn software (v. 1.13, Bruker-microCT) throughout the biofilm resulting in 10 different measurements. The mean thickness values were calculated as the arithmetic mean of the ten measurements. Three-dimensional models of dentin blocks and biofilms were acquired using CTVol v.2.2.1 (Bruker-microCT) software.

Statistical analysis

The differences between the groups regarding biofilm thickness measurements and viable and total cell density values were statistically analyzed using the Kruskal–Wallis one-way analysis of variance and Dunn’s tests after the Shapiro–Wilk test revealed the data were not normally distributed. The statistical significance level was established at 0.05, and SPSS 21.0 software (SPSS Inc, Chicago, IL, USA) was used for the statistical analyses.

Results

Transmission electron microscope analysis

Biofilm formation was detected on all dentin blocks. No comparison was made between groups 1 and 2 since similar photomicrographs were obtained in both groups. TEM photomicrographs showed that barium sulfate-penetrated biofilm structure and penetrated some of the observed bacterial cell walls (Fig. 3). Also, some of the bacteria cells were ruptured, while others remained intact. However, bacteria, which were not penetrated by barium sulfate, were also detected. Photomicrographs of the control group exhibited no barium sulfate within the cell and viable bacteria.

Confocal laser scanning microscopy findings

Viable cell density and total cell density values of the control group were similar to those of groups 1 and 2 ($P > 0.05$, Table 1). The concentration of barium sulfate also had no significant effect on the viable and total cell density values ($P > 0.05$).

Table 1 Mean and standard deviation (median) values of viable and total cell density of biofilm calculated from CLSM (AU)

Group	Viable cell density	Total cell density	N
Control group	3.98 ± 1.93 (3.94) ^a	11.06 ± 4.56 (9.77) ^a	3
50% barium sulphate group	2.32 ± 2.26 (1.41) ^a	9.03 ± 6.39 (6.42) ^a	5
100% barium sulphate group	2.61 ± 1.93 (1.55) ^a	8.52 ± 6.17 (5.98) ^a	5

Different superscript letters indicate statistically significant difference ($P < 0.05$)

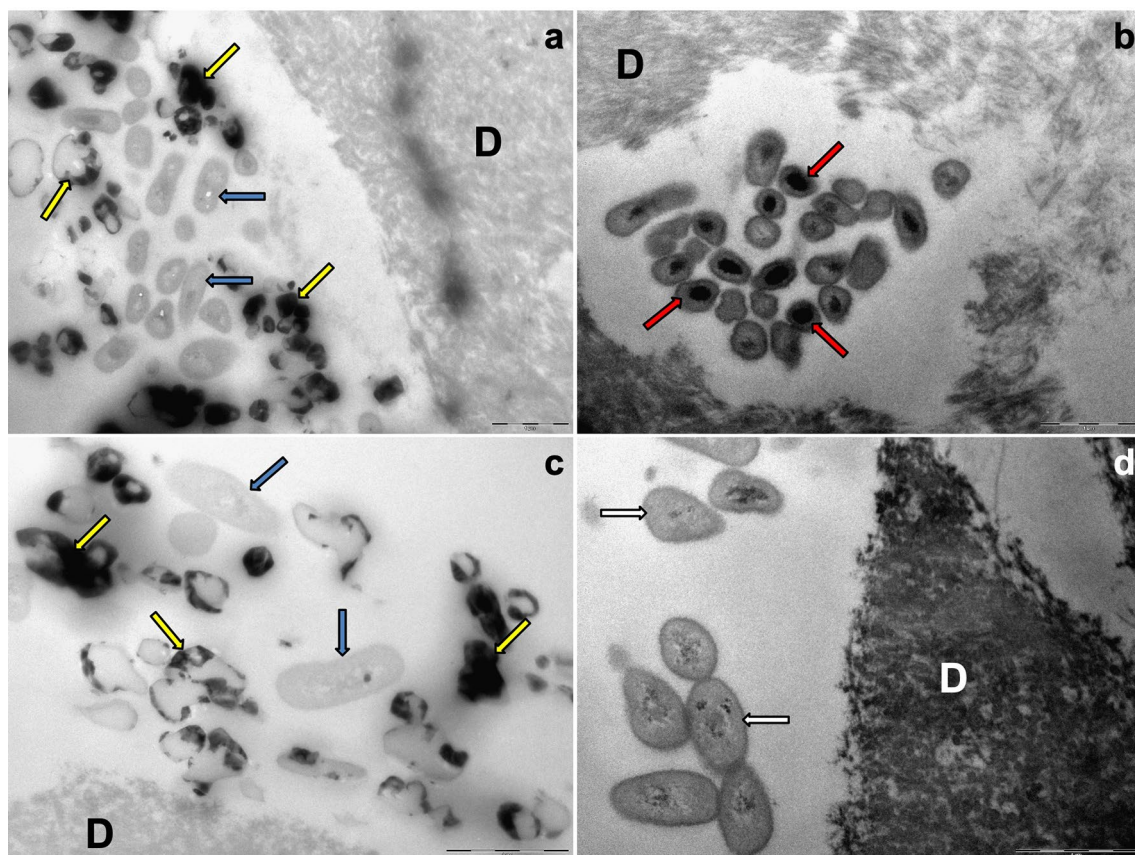


Fig. 3 **a**—Electron dense barium sulfate precipitate (yellow arrows) within and on the surface of bacteria cytoplasm with distorted integrity and shape (bacteria cell wall and membrane), bacteria with intact shape and integrity (blue arrows), dentin (D) TEM, $\times 12,500$. **b**—Electron dense barium sulfate precipitate (red arrows) in the intact bacterial cytoplasm. TEM, $\times 16,000$. **c**—Electron dense barium

sulfate precipitate (yellow arrows), intact and intact bacteria (blue arrows), dentin (D) in the cytoplasm and surface (bacterial cell wall and membrane) of impaired integrity and shape. TEM, $\times 20,000$. **d**—Bacteria with normal ultrastructural structure (white arrows), dentin (D). TEM was edited as $\times 20,000$

Micro-computed tomography analysis

No measurable biofilm structure was detectable on dentin blocks in the control group (Fig. 4a, d). An accumulated structure that was more radiopaque than dentin was evident in groups 1 and 2 (Fig. 4b, c, e). Kruskal–Wallis one-way analysis of variance test revealed no significant difference between different concentrations of barium sulfate regarding biofilm thickness ($P > 0.05$) (Table 2).

Discussion

Persistence of dental infections has been associated with the presence of biofilm communities rather than planktonic microorganisms (Costerton et al. 1999; Parsek and Singh, 2003). Therefore, compositional analysis, characterization, and three-dimensional visualization of biofilms are essential to understand the mechanisms responsible for the function of biofilms and their interaction with the environment (Miller et al. 2012). Developments in imaging technology have generated substantial data regarding the nature of biofilm. Various visualization techniques have been suggested to study biofilms, and quantitative evaluation and characterization of biofilm is still a developing subject (Alhede et al. 2012; Ivankovic et al. 2016; Schlafer and Meyer 2017).

TEM has been suggested to overcome the limitations of traditional scanning electron microscopy for the detection of the samples with greater detail and without the distortion of hydrated components (Reese and Guggenheim 2007). TEM presents high-resolution insight into the ultrastructure of the bacterial cells and extracellular polymeric matrix due to the

Table 2 Mean and standard deviation (median) values of biofilm thicknesses measured by micro CT (μm)

Barium sulphate concentration	Biofilm thickness	<i>N</i>
50% barium sulphate	5.91 ± 1.30 (5.85) ^a	10
100% barium sulphate	5.55 ± 0.81 (5.39) ^a	10

Different superscript letters indicate statistically significant difference ($P < 0.05$)

preparation of ultrathin samples despite extensive preparation steps (Hannig et al. 2010). In the present study, TEM was utilized to assess the interaction between barium sulfate and biofilm bacteria. Photomicrographs showed penetration of barium sulfate crystals into the deeper layers of biofilm. It was seen that some bacterial cells embodied barium sulfate crystals, but not all of them were penetrated by barium sulfate.

Moreover, TEM showed that some of the bacteria that embodied barium sulfate crystals were intact, whereas the cell walls of others seemed ruptured. A previous study utilized barium sulfate for biofilm staining; however, no TEM evaluation was used in that study (Davit et al. 2011). Therefore, direct comparisons cannot be made between the results of these studies regarding the TEM results. TEM images obtained from this study exhibited similar effects of barium sulfate application on biofilm components between groups 1 and 2, both presenting invasion of barium sulfate crystals into the deeper layers of biofilm as well as sound and ruptured bacterial cells. The ruptured cells may have occurred due to the chemical fixation and decalcification steps before TEM examination.

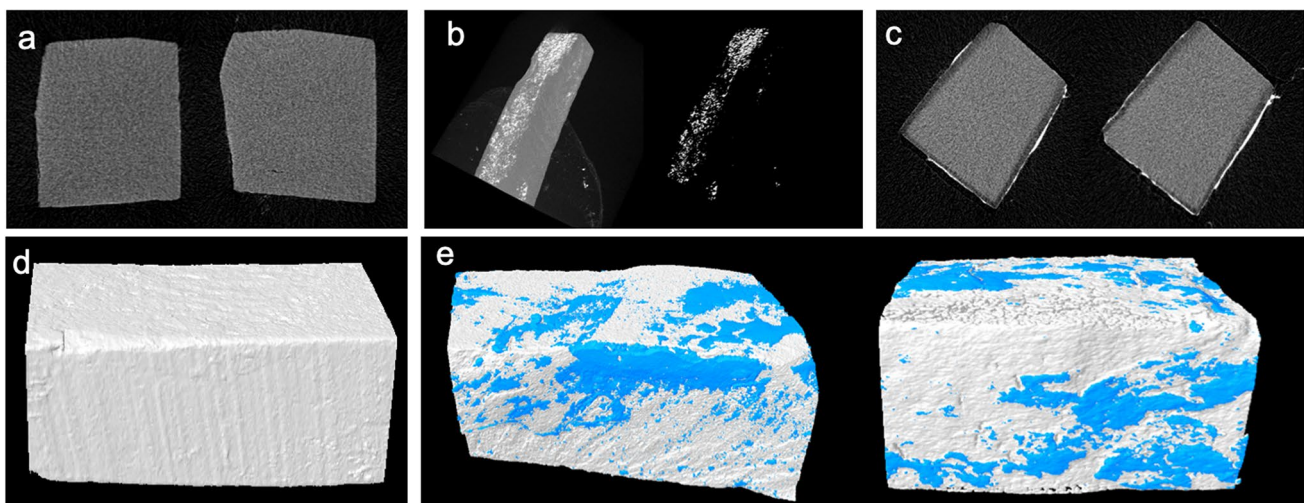


Fig. 4 The radiopacity of barium sulfate could not be detected in the control group (a, d). Visualization of the radiopacity of the biofilm structure formed on the dentin blocks during micro-CT scanning (b). The appearance of the biofilm structure in two-dimensional micro-

CT images (c). Three-dimensional micro-CT visualization of dentin blocks and biofilms (e) Biofilm is shown in blue, and dentin block is shown in white

CLSM may be used to evaluate the effect of different treatment regimens on biofilm structure. This technique produces images with less resolution than SEM but allows the determination of biofilm biomass, biovolume, and cell distribution quantitatively. In the present study, CLSM was performed for each group to measure viable and total cell density before and after the barium sulfate application. Interestingly, no significant difference was found between barium sulfate-treated and control groups regarding viable and total cell densities, although TEM images showed ruptured bacterial cells. It was contradictory for TEM and CLSM results to show similar viable cell density since all bacterial cells seemed intact in the control group under the TEM examination. This could be attributed to 2-dimensional sectional photomicrographs generated by TEM with no quantitative information regarding cell density of the entire biofilm structure. Moreover, the total duration of interaction between barium sulfate and biofilm might also influence cell viability.

Both TEM and CLSM require ultrathin specimen preparation to expose biofilm structure to be visualized. Micro-CT has the advantage of penetrating the dental tissues to show its inner root canal anatomy with great detail without necessitating a preparation step. Reproducible techniques that allow operators to characterize biofilm structure quantitatively with regard to its thickness, density, and volume might be useful to study the effect of elimination techniques on biofilm structure (Heydorn et al. 2000). The present study proposes a novel technique to visualize biofilm using micro-CT technology. The presented results showed that biofilm structure, in which the barium sulfate invasion was confirmed with TEM, could be visualized three-dimensionally using micro-CT. Moreover, the biofilm thickness could also be measured. Therefore, the null hypothesis that micro-CT was efficient to visualize biofilm structure formed on dentin was accepted.

A recent micro-CT study used dual-energy and quantitatively analyzed biofilm volume data by subtracting two different scanning data obtained with dual-energy acquisition (Pires et al. 2018). This technique provided visualization of biofilm structure without prior application of any contrasting agent; however, the technique was also reported to be dependent on cavity dimensions (Pires et al. 2018). Biofilm could also be differentiated in a single micro-CT scanning if the contrasting agents are used. A previous study showed that barium sulfate penetrated the deep layers of biofilm and provided radiopaque images (Davit et al. 2011). In agreement, the present study showed that both 50% and 100% concentrations of barium sulfate had been determined as adequate to visualize biofilm structure with micro-CT. Dentin is also a radiopaque structure; thus, it is important to differentiate between radiopacities of biofilm and dentin. This study showed that the application of both 50% and 100% barium sulfate provided biofilm structure to have a more radiopaque image compared to dentin. The

difference between dentin and biofilm structure regarding their radiopacity favored the visualization and measurement of biofilm using micro-CT.

Micro-CT eliminates the preparation process and provides the specimen to be reused to examine the efficacy of disinfection protocols. In the present study, both TEM and CLSM examinations exhibited dead bacterial cells after barium sulfate application. On the other hand, the micro-CT technique provided no information regarding the viability of cells or inner cell structures, such as organelles, which constituted the limitations of the present technique.

Pires et al. (2018) calculated the volume of biofilm formed in artificial dentin cavities using dual-energy micro-CT. In the present study, biofilm thickness was measured at ten different points of the biofilm structure since biofilms showed irregular outlines. Previous studies reported that biofilm thickness of *E. faecalis* could increase up to 25.5 μm (Pei et al. 2012; Periasamy et al. 2012). These values might differentiate between studies due to variations, e.g., incubation duration and choice of substrate, and they can be easily visualized during micro-CT scanning with 2.5 μm resolution. The results of the present study showed that biofilm thickness was not affected by the barium sulfate concentration. The thicknesses of the detected biofilms were 5–6 μm . These results were similar to those reported by Chandra et al. (2015), in their study on CLSM examination of *E. faecalis* biofilm; however, methodological differences between studies prevent direct comparison of the results.

In this study, after applying barium sulfate, dentin blocks were washed three times and then micro-CT scan was performed. However, the barium sulfate deposits that adhered to dentin surface may have caused a radiopaque image without biofilm presence. In micro-CT imaging, this possible radiopaque deposit, which does not contain biofilm, may have been evaluated as biofilm. In particular, a thin irregular radiopaque layer can be seen around the dentin block in Fig. 4c. The actual justification for the formation of such irregular dense structure could not definitely be made; however, it could cause from a possible demineralization effect of biofilm on dentin surface or beam-hardening artifact. Another possible limitation of the presented technique was the use of 2.5 μm resolution value, which required 1 h of processing time for $1 \times 4 \times 1$ mm dentin blocks. Such scanning parameters would cause a total of 3 h scanning duration for an actual root. To shorten this duration, splitting root canals into parts to focus, and the use of 2.5 μm voxel size is suggested.

Conclusion

This study proposed a reproducible and quantitative method to visualize and measure biofilm structure and could serve as a basis for further analysis. The efficacy of disinfection

techniques and materials to remove biofilm structure within root canals could be evaluated by quantitative analysis of biofilm thickness. Biofilm thicknesses could be measured before and following the application of tested disinfection protocols on experimentally infected root canals by two micro-CT scanning, and the difference between the biofilm thicknesses could reflect the efficacy of tested protocols. Further studies should evaluate the ability of barium sulfate to penetrate the biofilm structure formed in actual root canals.

Author contributions AK: Conceptualization, Methodology, Investigation, Data Curation, Writing — Original Draft, Visualization, Supervision, Funding Acquisition. CK: Methodology, Investigation, Data analysis, Writing — Review and Editing. MK: Methodology, Investigation, Data Curation, Writing. YY: Investigation, Resources, Visualization, Supervision, Funding Acquisition, Review and Editing. MG: Validation, Visualization, Supervision, Funding Acquisition, Writing — Review and Editing. HA: Validation, Visualization, Supervision, Funding Acquisition, Writing — Review and Editing. FŞ: Conceptualization, Methodology, Validation, Writing — Review and Editing.

Funding This study was supported by the Scientific and Technological Research Council of Turkey-TUBITAK (Grant no. 114S511).

Compliance with ethical standards

Conflict of interest Ali Keleş and Cangül Keskin have a pending patent application from Turkish National Patent Office. Authors deny any conflicts of interest.

Human rights and informed consent This article does not contain any studies with human performed by any of the authors.

References

- Alhede M, Qvortrup K, Liebrechts R, Høiby N, Givskov M, Bjarnsholt T (2012) Combination of microscopic techniques reveals a comprehensive visual impression of biofilm structure and composition. *FEMS Immunol Med Microbiol* 65:335–342. <https://doi.org/10.1111/j.1574-695X.2012.00956.x>
- Bergmans L, Moisiadis P, Van Meerbeek P, Quirynen M, Lambrechts P (2005) Microscopic observation of bacteria: review highlighting the use of environmental SEM. *Int Endod J* 38:775–788. <https://doi.org/10.1111/j.1365-2591.2005.00999.x>
- Carrel M, Morales VL, Beltran MA, Derlon N, Kaufmann R, Morgenroth E, Holzner M (2018) Biofilms in 3D porous media: Delineating the influence of the pore network geometry, flow and mass transfer on biofilm development. *Water Res* 134:280–291. <https://doi.org/10.1016/j.watres.2018.01.059>
- Chandra PVR, Kumar VH, Reddy SJ, Kiran DR, Krishna MN, Kumar GV (2015) Biofilm forming capacity of *Enterococcus faecalis* on Gutta-percha points treated with four disinfectants using confocal scanning laser microscope: an in vitro study. *Dent Res J (Isfahan)* 12:331–336. <https://doi.org/10.4103/1735-3327.161446>
- Costerton JW, Stewart PS, Greenberg EP (1999) Bacterial biofilms: a common cause of persistent infections. *Science* 284:1318–1322. <https://doi.org/10.1126/science.284.5418.1318>
- Costerton JW, Montanaro L, Arciola CR (2005) Biofilm in implant infections: its production and regulation. *Int J Artif Organs* 28:1062–1068. <https://doi.org/10.1177/0391398805022801103>
- Davit Y, Iltis G, Debenest G, Veran-Tissoires S, Wildenschild D, Gérino M, Quintard M (2011) Imaging biofilm in porous media using X-ray computed microtomography. *J Microsc* 242:15–25. <https://doi.org/10.1111/j.1365-2818.2010.03432.x>
- Du T, Wang Z, Shen Y, Ma J, Cao Y, Haapasalo M (2014) Effect of long-term exposure to endodontic disinfecting solutions on young and old *Enterococcus faecalis* biofilms in dentin canals. *J Endod* 40:509–514. <https://doi.org/10.1016/j.joen.2013.11.026>
- Flemming HC, Wingender J (2010) The biofilm matrix. *Nat Rev Microbiol* 8:623–633. <https://doi.org/10.1038/nrmicro2415>
- Hannig C, Follo M, Hellwig E, Al-Ahmad A (2010) Visualization of adherent microorganisms using different techniques. *J Med Microbiol* 59:1–7. <https://doi.org/10.1099/jmm.0.015420-0>
- Heydorn A, Nielsen AT, Hentzer M, Sternberg C, Givskov M, Ersbøll BK, Molin S (2000) Quantification of biofilm structures by the novel computer program COMSTAT. *Microbiology* 146:2395–2407. <https://doi.org/10.1099/00221287-146-10-2395>
- Ivankovic T, du Roscoat SR, Geindreau S, Séchet C, Huang P, Martins JM (2016) Development and evaluation of an experimental protocol for 3-D visualization and characterization of the structure of bacterial biofilms in porous media using laboratory X-ray tomography. *Biofouling* 32:1235–1244. <https://doi.org/10.1080/08927014.2016.1249865>
- Kreth J, Herzberg MC (2015) Molecular principles of adhesion and biofilm formation. In: Chavez de PL, Sedgley C, Kishen A (eds) *The root canal biofilm*, 1st edn. Springer Series on Biofilms, vol. 9. Springer, Berlin, Heidelberg, pp 23–53
- Miller EA, Xiao X, Miller X, Keller MP, White TA, Marshall M (2012) Investigating biofilm structure using X-ray microtomography gratings-based phase contrast. *Proc. SPIE* 8506, Developments in X-Ray Tomography VIII, 85061H (17 October 2012). <https://doi.org/10.1117/12.930105>
- Ordinola-Zapata R, Bramante C, Versiani M, Moldauer B, Topham G, Gutmann J, Nuñez A, Duarte M, Abella F (2017) Comparative accuracy of the clearing technique, CBCT and micro-CT methods in studying the mesial root canal configuration of mandibular first molars. *Int Endod J* 50:9096. <https://doi.org/10.1111/iej.12593>
- Parsek MR, Singh PK (2003) Bacterial biofilms: an emerging link to disease pathogenesis. *Ann Rev Microbiol* 57:677–701. <https://doi.org/10.1146/annurev.micro.57.030502.090720>
- Plouraboue F, Cloetens P, Fonta C, Steyer A, Lauwers F, Marc-Vergnes J (2004) X-ray high-resolution vascular network imaging. *J Microsc* 215:139–148. <https://doi.org/10.1111/j.1365-2818.2010.03432>
- Pei X, Lu X, Liu J, Liu D, Yang Y, Ostrikov K, Chu PK, Pan Y (2012) Inactivation of a 25.5 µm *Enterococcus faecalis* biofilm by a room-temperature, battery-operated, handheld air plasma jet. *J Phys D Appl Phys* 45:165205. <https://doi.org/10.1088/0022-3227/45/16/165205>
- Periasamy S, Joo HS, Duong AC, Bach THL, Tan VY, Chatterjee SS, Cheung GY, Otto M (2012) How *Staphylococcus aureus* biofilms develop their characteristic structure. *Proc Natl Acad Sci* 109:1281–1286. <https://doi.org/10.1073/pnas.1115006109>
- Pires PM, dos Santos TP, Fonseca-Gonçalves A, Pithon MM, Lopes RT, de Almeida Neves A (2018) A dual-energy micro-CT methodology for visualization and quantification of biofilm formation and dentin demineralization. *Arch Oral Biol* 85:10–15. <https://doi.org/10.1016/j.archoralbio.2017.09.034>
- Reese S, Guggenheim B (2007) A novel TEM contrasting technique for extracellular polysaccharides in in vitro biofilms. *Microsc Res Tech* 70:816–822. <https://doi.org/10.1002/jemt.20471>
- du Roscoat SR, Martins J, Séchet P, Vince E, Latil P, Geindreau C (2014) Application of synchrotron X-ray microtomography for

- visualizing bacterial biofilms 3D microstructure in porous media. *Biotechnol Bioeng* 111:1265–1271. <https://doi.org/10.1002/bit.25168>
- Rosen E, Tsesis I, Elbahary S, Storzi N, Kolodkin-Gal I (2016) Eradication of *Enterococcus faecalis* biofilms on human dentin. *Front Microbiol* 7:2055. <https://doi.org/10.3389/fmicb.2016.02055>
- Schlafer S, Meyer RL (2017) Confocal microscopy imaging of the biofilm matrix. *J Microbiol Methods* 138:50–59. <https://doi.org/10.1016/j.mimet.2016.03.002>
- Stewart PS, Costerton JW (2001) Antibiotic resistance of bacteria in biofilms. *Lancet* 358:135–138. [https://doi.org/10.1016/S0140-6736\(01\)05321-1](https://doi.org/10.1016/S0140-6736(01)05321-1)

Publisher's Note Springer Nature remains neutral with regard to jurisdictional claims in published maps and institutional affiliations.